14. Site-directed mutagenesis was used to (i) change the α initiation codon from ATG to CTG, (ii) change the αCys[193] to Ser, (iii) change the γSer[107] to Cys, (iv) change the γ initiation codon from GTG to ATG, and (v) change the γ termination codon from TAG to TAA in the cloned F_1-ATPase construct (pGEM-DEMH). The construct also contained a 10-histidine tag that was inserted immediately downstream of the β initiation codon. The recombinant protein was expressed in *E. coli* JM103 Δ(*uncB-uncD*) and purified using affinity (i.e., Ni–nitrilotriacetic acid) and size exclusion chromatography.
15. T. Matsui, M. Yoshida, *Biochim. Biophys. Acta* **1231**, 139 (1995).
16. The exposure pattern written on the cover slip consisted of dots with a 5-μm horizontal and vertical pitch and border marks to identify the post region. The dots averaged 50 to 120 nm in diameter, depending on the e-beam exposure dose, which varied from 10 to 30 fC/μm². The exposed area measured 300 μm by 300 μm, exclusive of the border marks. The border marks (lines 50 μm wide) were spaced 0.5 μm from the edge of the post region.
17. The patterning was performed on silicon wafers that were spin-coated with 4% PMMA in methoxybenzene at 3000 rpm, resulting in a thickness of ~150 nm. The width of the nanopropellers was 150 nm; their length varied from 750 nm to 1.4 μm, depending on the exposure dose, which varied from 3.75 to 4.5 nC/cm. The optimum dose was determined to be 4.3 nC/cm.
18. The synthetic His-rich peptide was specifically biotinylated to the NH_2-terminal Cys residue through disulfide linkage in the presence of *N,N*-dimethylformamide. A 100-μl aliquot of the biotinylated peptide was incubated with 400 μl of the nanopropellers for 15 min, then dialyzed against 1× PBS to remove any excess peptide and biotin maleimide.
19. D. J. Jeffrey, Y. Onishi, *J. Mech. Appl. Math.* **34**, 129 (1981).
20. A. J. Hunt, F. Gittes, J. Howard, *Biophys. J.* **67**, 766 (1994).
21. L. Stryer, *Biochemistry* (Freeman, New York, ed. 4, 1999), pp. 445–447.
22. H. Omote *et al.*, *Proc. Natl. Acad. Sci. U.S.A.* **96**, 7780 (1999).
23. H. Noji *et al.*, *Biochem. Biophys. Res. Commun.* **260**, 597 (1999).
24. T. Hisabori, A. Kondoh, M. Yoshida, *FEBS Lett.* **463**, 35 (1999).
25. We thank F. Peters for figure preparation and assistance in digitization of the data. Supported by grants from the Keck Fellowship Program, Office of Naval Research, and Defense Advanced Research Projects Agency (N00014-99-1-0436CS), NSF (ECS-9007033 and ECS-7876771), U.S. Department of Energy (DE-FG07-96ER14703), and NASA (NAG5-8775).

1 August 2000; accepted 13 October 2000

Mechanisms of Ordering in Striped Patterns

Christopher Harrison,[1] Douglas H. Adamson,[2] Zhengdong Cheng,[1]* John M. Sebastian,[3] Srinivasan Sethuraman,[4] David A. Huse,[1] Richard A. Register,[3] P. M. Chaikin[1]

We have studied the ordering dynamics of the striped patterns of a single layer of cylindrical block copolymer microdomains in a thin film. By tracking disclinations during annealing with time-lapse atomic force microscopy, we observe a dominant mechanism of disclination annihilation involving three or four disclinations (quadrupoles). Pairwise disclination annihilation events are suppressed as a result of the topological constraints in this system. The kinetic scaling laws with exponents observed here are consistent with topologically allowed annihilation events involving multiple disclinations. The results provide insight into two-dimensional pattern formation and may lead to the successful application of block copolymer lithography.

Striped patterns are produced in a variety of disparate systems, including Rayleigh-Benard convection cells, ferrimagnetic films with dipolar interactions, and biological development such as with a zebra's stripes, or perhaps closer at hand, in one's fingerprints (*1*). A classic realization of a nondriven striped system is the two-dimensional (2D) smectic liquid crystal. This system has been the focus of intense research since being discussed by several seminal articles two decades ago (*2*). Although there has been recent progress in understanding equilibrium phenomena such as the role of orientational and translational order in 2D smectics (*3*, *4*), little is known about the kinetics and mechanisms by which order evolves in a 2D smectic system after being quenched from the disordered state, although this has been explored by simulations (*5–8*). The most pressing application for understanding pattern formation in 2D smectics is block copolymer lithography—a process that uses self-assembled patterns (such as single layers of cylinders or spheres) as a template to fabricate devices at the nanometer-length scale (*9–11*). Therefore, our motivation is both fundamental understanding of pattern coarsening and optimization of microdomain order for copolymer lithography, an application that has been used to produce an unprecedented density of metal dots for information storage (*12*), and most recently, to fabricate InGaAs/GaAs quantum dots for laser emission (*13*). We show that the coarsening process is driven by the interaction of topological defects and that the measured kinetic exponents can be understood in terms of a dominant annihilation mechanism that involves more than two disclinations.

Our model system consists of microphase separated block copolymers in thin films. Block copolymers consist of two or more homogeneous but chemically distinct blocks that have been connected with a covalent bond (*14*). Microphase separation produces morphologies largely set by the volume fraction, such as lamellae, cylinders, or spheres. Although these fundamental morphologies have been well studied for decades, the factors that determine the range of orientational and translational order (grain size) are not well understood. The coarsening kinetics in three dimensions have been studied (*15–17*), but no mechanistic understanding of the ordering process has been developed, partly owing to lack of data on the real-space dynamics during pattern development, which is our focus here.

A polystyrene-polyisoprene (PS-PI) diblock was synthesized by means of living anionic polymerization with masses of 30 and 11 kg/mol for the PS and PI blocks (SI 30-11) to produce PI cylinders in a PS matrix. This diblock was applied to carbon-coated silicon substrates by spin coating from a dilute solution, and order was induced through vacuum annealing (Fig. 1A) (*18*). A representative image from a similar system shows cylinders (lighter) lying parallel to the substrate (Fig. 1B). Because samples sizes were on the order of square centimeters, there were at least 10^5 microdomain repeat spacings in any direction, thereby negating edge effects. After annealing, microdomains were preferentially stained with the vapors of OsO_4 to provide contrast for a Zeiss 982 scanning electron microscope (SEM) (*18–20*). The SEM allowed us to image large areas of the polymer film at high resolution for accurate measurements of the average grain size.

The orientational correlation length (ξ_2) of the pattern was measured as a function of annealing time to quantitatively characterize the degree of microdomain order. This was accomplished by collecting many SEM images of each sample and computationally measuring the local orientational order parameter, $\psi(\vec{r}) = \exp[2i\theta(\vec{r})]$, where $\vec{r}$ is position and θ is the microdomain or stripe orientation (similar to director) (*21*). The azimuthally averaged correlation function $g_2(r) = \langle\psi(0)\psi(r)\rangle$ was then calculated and the correlation length ξ_2 was measured by fitting $g_2(r)$ with e^{-r/ξ_2}. Two annealing temperatures (413 K and 443 K) were examined

[1]Department of Physics, [2]Princeton Materials Institute, [3]Department of Chemical Engineering, Princeton University, Princeton, NJ 08544, USA. [4]Jet Propulsion Laboratory, 4800 Oak Grove Drive, Mailstop 302-306, Pasadena, CA 91109, USA.

*Present address: ExxonMobil Research and Engineering Company, 1545 Route 22 East, Annandale, NJ 08801–0998, USA.

to yield the correlation lengths (Fig. 2A). A best-fit power law of $\xi_2(t) \sim t^{0.25 \pm 0.02}$ is measured at 443 K and $\xi_2(t) \sim t^{0.25 \pm 0.02}$ is measured at 413 K, suggesting a fractional kinetic exponent of 1/4.

To understand the driving force for this coarsening process, we studied the role of topological defects (*22*, *23*). We first measured the densities $\rho_{\pm}$ of $\pm 1/2$ disclinations (Fig. 1B) as a function of time and temperature. Using the same data sets as discussed above, we plot the time dependence of $\rho_{+}^{-1/2}$ and $\rho_{-}^{-1/2}$, the average distance between disclination cores (pointlike here) of the respective signs (Fig. 2B). The interdisclination spacing can be seen to increase with the same power law as $\xi_2(t)$, confirming that $\rho \sim \xi_2^{-2}$. The magnitudes of $\xi_2(t)$ and $\rho(t)^{-1/2}$ are within a geometrical factor of each other (about 2), confirming that the orientational order of the sample is dominated by orientational defects. The similar values of $\rho_{+}^{-1/2}$ and $\rho_{-}^{-1/2}$ throughout the experiment suggest that annihilation of disclinations of opposite sign is occurring, driving the growth of ξ_2.

Although SEM was used for the most accurate measurements of the correlation lengths, the necessary OsO_4 staining arrests all polymer dynamics. Therefore, to observe the motion of individual defects, we used a nondestructive imaging technique that took advantage of the modulus difference between the two blocks for tapping mode atomic force microscopy (Nanoscope IIIa AFM, Digital Instruments) (*24*). To minimize degradation during annealing in the AFM, we synthesized another PS-PI diblock, and the polyisoprene block was hydrogenated to poly(ethylene-alt-propylene) (*25*). This diblock, denoted SEP 5-13, forms PS cylinders in a PEP matrix, the morphological inverse of SI 30-11. The spin-coated sample was imaged at ambient temperature, annealed in air on a temperature-controlled heater stage mounted on the AFM, and then reimaged after cooling to examine the coarsened microdomain pattern. By repeating this cycle dozens of times and reimaging the same area, we observed the annihilation processes of disclinations [see Web movie entitled "Ordering of Striped Pattern" (*26*)].

Topological constraints dictate the favorability of various possible coarsening mechanisms. For smectic systems, a disclination pair (such as shown in Fig. 1B) has an associated Burgers vector (*27*) with magnitude equal to twice the separation distance. As the Burgers vector is conserved, the annihilation of a disclination pair produces a number of like-charged dislocations equal to the original Burgers vector divided by the layer spacing d (Fig. 1). Although dislocations shed in this process can annihilate with other oppositely oriented dislocations, this is less favorable than a process that produces few or no dislocations. Consequently, we rarely observe this coarsening mechanism for disclination pairs separated by more than a few layers. In contrast, the mutual annihilation of two pairs of disclinations forming a quadrupole, where each pair has an oppositely oriented Burgers vector of similar magnitude, reduces the net production of dislocations [Fig. 3 and Web movie entitled "Quadrupole Annihilation" (*26*)]. Quadrupole annihilation events were observed about 10 times as often as dipole events and at all stages of the coarsening process (all length scales).

We now discuss the origin of the measured kinetic exponents using the above mechanism of coarsening as a guide. The essential topological constraint on the evolution of these stripe patterns is that disclination motion requires the production or absorption of dislocations, lowering the kinetic exponent from that observed in nematic systems (1/2) (*28*, *29*). Pattern coarsening will progress if the free energy is being reduced. Processes involving the creation of fewer dislocations are favored because each costs a core energy. Thus, the annihilation of a pair of disclinations alone is rarely seen because this requires transforming the Burgers vector into dislocations. Multidisclination annihilations are more favorable because a third disclination can act as a source or sink of dislocations, relieving the topological constraint and allowing an oppositely charged pair of disclinations to approach and annihilate. Alternatively, a set of four disclinations can be arranged so they have no net Burgers vector (Fig. 3A, inset); these four may then mutually annihilate without net production of dislocations. Only about one-half of all disclination annihilations could be characterized in our experiments; of these, almost all involved tripoles or quadru-

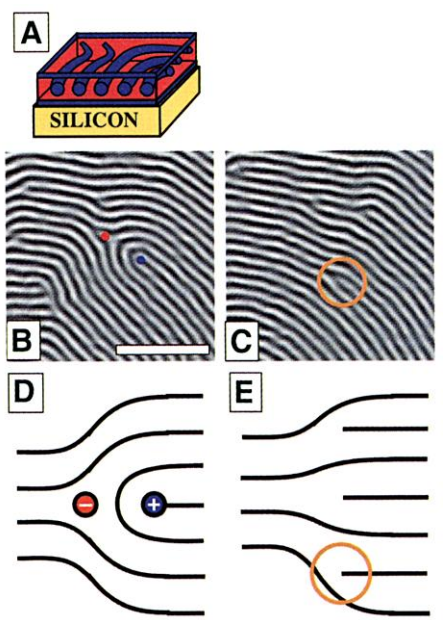

Fig. 1. (**A**) Schematic of one layer of polyisoprene cylinders (blue) in a polystyrene matrix (red) on a silicon substrate. Polyisoprene layers wet the air and substrate surfaces. (**B**) AFM image of a disclination dipole (Burgers vector 6*d*, +1/2 disclination indicated by the blue circle, −1/2 disclination by the red circle), plus six additional dislocations, three each of the two orientations. Bar, 200 nm. (**C**) The dipole has annihilated after further annealing. Four dislocations (one example indicated with the orange circle) of the orientation corresponding to the dipole's original Burgers vector remain in the field of view. Additional dislocations have diffused out of the image area. This process was observed infrequently. (**D** and **E**) Schematic of disclination dipole annihilation with Burgers vector 3*d*. The strain fields cause the disclinations to annihilate, producing three dislocations (one example indicated with the orange circle) after annihilation in (E).

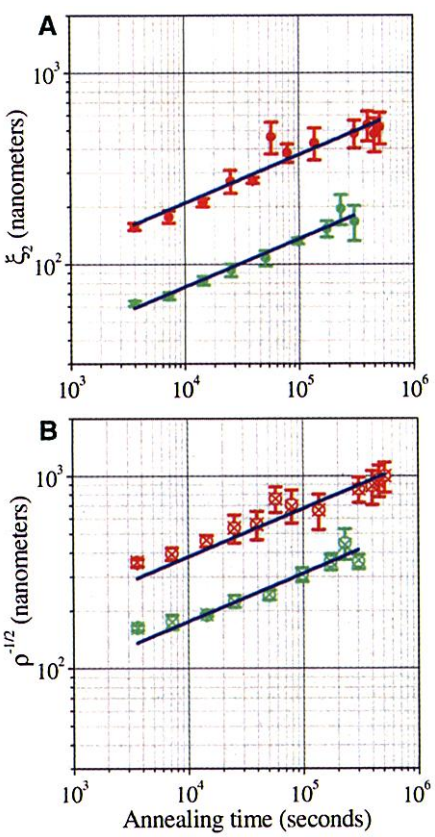

Fig. 2. (**A**) Orientational correlation length for cylindrical microdomains (SI 30-11) as a function of time. The red data (top) correspond to 443 K and the green (bottom) to 413 K. The solid blue lines are power-law fits to the data, yielding the kinetic exponents of 0.25 ± 0.02 at 443 K and 0.25 ± 0.02 at 413 K. (**B**) The average spacing between disclinations as a function of annealing time for the same data sets as shown in (A). The interdefect spacing was measured from $\rho_{\pm}^{-1/2}$, where $\rho_{\pm}$ is the disclination density of the respective sign. Because of their similar magnitudes, the data points for $\rho_{+}^{-1/2}$ (open circles) predominantly lie directly on those for $\rho_{-}^{-1/2}$ (crosses). For both annealing temperatures, the correlation length increases with a power law similar to that for the interdisclination spacing, implying that disclination annihilation dominates the coarsening process. The solid blue lines are power laws with exponents of 1/4.

poles, leading us to consider associated annihilation mechanisms to motivate the measured kinetic exponents.

For concreteness, consider a disclination quadrupole where the average separations are r. This discussion pertains equally to a disclination dipole and a nearby single disclination, where the unpaired disclination acts as a sink to absorb the dislocations produced by the collapse of the dipole. Oppositely charged disclinations attract with a potential varying as $\ln(r)$. This produces forces on the disclinations varying as $1/r$. However, the disclinations cannot simply move in response to these forces, owing to the topological constraint. Let us assume that the elementary step that allows a pair of $\pm 1/2$ disclinations to move together by one layer requires the motion of a dislocation from one disclination pair to another. Thus, a dislocation must move a distance r in order for the disclinations to move only one unit. The resulting decrease in the free energy of the disclination strain field is on the order of $\Delta E \sim 1/r$. The force f driving the dislocation's motion is the energy change divided by the distance traveled r, $f \sim \Delta E/r \sim 1/r^2$ (naïvely). If we assume that the dislocation motion is viscous with speed proportional to force, the dislocation's speed is $v \sim 1/r^2$. Because the dislocation has to travel a distance r, the time for this process (the net result of which is only one unit of disclination motion dr) is $dt \sim r/v \sim r^3$. Thus, the disclinations move toward one another as $-dr/dt \sim 1/r^3$, yielding $r \sim (t_f - t)^{1/4}$, where t_f is the time when they annihilate. This scenario suggests that the typical spacing between the remaining disclinations at time t grows as $\xi(t) \sim t^{1/4}$, consistent with our measured exponent in Fig. 2A.

In summary, we have demonstrated that a 2D smectic system has additional topological constraints (dictated by periodic translational order and hence conservation of Burgers vector) that lower the kinetic exponents to 1/4 from the value of 1/2 observed in 2D nematic systems. Pattern coarsening occurs predominantly by an annihilation process involving more than two disclinations such that a minimum number of dislocations is produced. Although this is the first suitable experimental system for studying 2D smectic pattern coarsening on length scales that are large compared with the layer spacing, the coarsening of layered or striped systems has been well explored by simulations during the past decade. Though earlier simulations focused on the nonconserved dynamics of Rayleigh-Benard cells, (*5*–*7*), recent work has established the applicability of this work to smectic or diblock copolymer systems where the dynamics are governed by a conserved density field. (*8*) Simulations produce kinetic exponents that are in agreement with our measurements, but have left open the physical mechanism. Our results suggest that the exponent results from disclination annihilation with the exchange of dislocations between disclination pairs relieving the particular topological constraints of striped systems. This points the way to a more rigorous understanding of pattern coarsening.

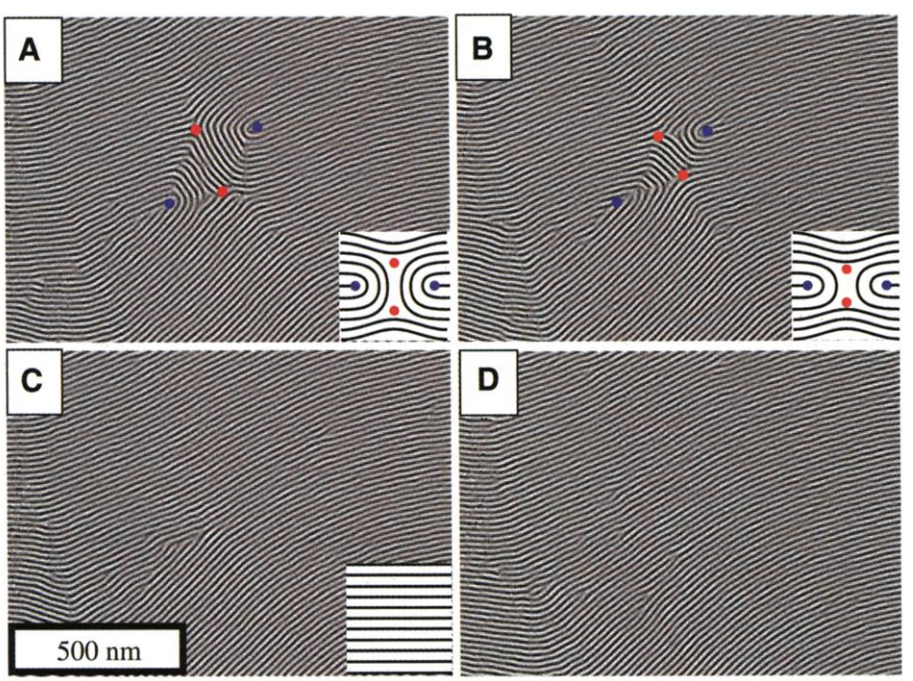

Fig. 3. AFM images taken from a sequence showing annihilation of a disclination quadrupole (+1/2 disclinations, blue; −1/2 disclinations, red) during annealing at 368 K. The schematics (**inset**) show an idealized quadrupole configuration analogous to each step. (**A**) After annealing for 34 min at 368 K, the spacing between +1/2 disclinations is about 17 layers, slightly less for the −1/2 disclinations. (**B**) After further annealing, the separation distances are reduced and the quadrupole has a Burgers vector of about 5*d*, depending on the exact location of the chosen path. Subsequent panels are obtained with 1-min intervals of annealing. (**C**) The quadrupole has annihilated, leaving a cluster of about four dislocations. This cluster can best be seen by viewing the image at an oblique angle parallel to the stripes. (**D**) Dislocations repel and separate.

References and Notes

1. C. Bowman, A. C. Newell, *Rev. Mod. Phys.* **70**, 289 (1998).
2. J. Toner, D. R. Nelson, *Phys. Rev. B* **23**, 316 (1981).
3. K. J. Strandberg, *Rev. Mod. Phys.* **60**, 161 (1988).
4. M. Seul, D. Andelman, *Science* **267**, 476 (1995).
5. Q. Hou, N. Goldenfeld, *Physica A* **239**, 219 (1997).
6. M. C. Cross, D. I. Meiron, *Phys. Rev. Lett.* **75**, 2152 (1995).
7. K. R. Elder, J. Vinals, M. Grant, *Phys. Rev. Lett.* **68**, 3024 (1992).
8. J. J. Christensen, A. J. Bray, *Phys. Rev. E* **58**, 5364 (1998).
9. M. Park, C. Harrison, P. M. Chaikin, R. A. Register, D. H. Adamson, *Science* **276**, 1401 (1997).
10. C. Harrison, M. Park, P. M. Chaikin, R. A. Register, D. H. Adamson, *J. Vac. Sci. Technol. B.* **16**, 544 (1998).
11. W. A. Lopes, H. M. Jaeger, *Bull. Am. Phys. Soc.* **44**, 1473 (1999).
12. M. Park, P. M. Chaikin, R. A. Register, D. H. Adamson, in preparation.
13. R. R. Li *et al.*, *Appl. Phys. Lett.* **76**, 1689 (2000).
14. F. S. Bates, G. H. Fredrickson, *Annu. Rev. Phys. Chem.* **41**, 525 (1990).
15. H. J. Dai, N. P. Balsara, B. A. Garetz, M. C. Newstein, *Phys. Rev. Lett.* **77**, 3677 (1996).
16. K. Amundson, E. Helfand, X. Quan, S. D. Hudson, S. D. Smith, *Macromolecules* **27**, 6559 (1994).
17. K. Amundson, E. Helfand, *Macromolecules* **26**, 1324 (1993).
18. C. Harrison *et al.*, *Polymer* **30**, 2733 (1998).
19. S. M. Sze, in *VLSI Technology* (McGraw-Hill, New York, ed. 2, 1988), pp. 184–232.
20. C. Harrison, M. Park, P. M. Chaikin, R. A. Register, D. H. Adamson, *Macromolecules* **31**, 2185 (1998).
21. The details of our computational techniques can be found in the thesis of C. Harrison (Princeton University, 1999) and in C. Harrison *et al.*, *Macromolecules* **33**, 857 (2000).
22. M. Kleman, *Points, Lines and Walls* (Wiley, New York, 1983).
23. P. G. de Gennes and J. Prost, *The Physics of Liquid Crystals* (Oxford Science Publications, New York, ed. 2, 1993).
24. J. Hahm, W. A. Lopes, H. M. Jaeger, S. J. Sibener, *J. Chem. Phys.* **109**, 10111 (1998).
25. J. L. Adams, D. J. Quiram, W. W. Graessley, R. A. Register, G. R. Marchand, *Macromolecules* **31**, 201 (1998).
26. Supplementary data are available at *Science* Online at www.sciencemag.org/cgi/content/full/290/5496/1558/DC1.
27. The Burgers vector construction is performed on a closed loop path integral and equals the net number of dislocations inside multiplied by the layer spacing. For a full description, see (*22*) or (*23*).
28. B. Yurke, A. N. Pargellis, T. Kovacs, D. A. Huse, *Phys. Rev. E.* **47**, 1525 (1993).
29. C. Liu, M. Muthukumar, *J. Chem. Phys.* **106**, 7822 (1997).

30. We gratefully acknowledge the support of M. Rooks, D. Carr, and G. Nagy at the Cornell Nanofabrication Facility where electron microscopy was performed. AFM was made possible by the efforts of S. Maganov, N. Yao, and J. Woodruff. We are indebted to Y. Xiao for computational assistance. We gratefully acknowledge useful discussions with D. Nelson and S. Milner. Supported by the National Science Foundation through the Princeton Center for Complex Materials (DMR-9400362 and DMR-9809483) and through DMR-9802468, and through the donors of the American Chemical Society Petroleum Research Fund (35207-AC5,7).

2 August 2000; accepted 16 October 2000